Biomedicine & Pharmacotherapy 167 (2023) 115559

Contents lists available at ScienceDirect

Biomedicine & Pharmacotherapy

journal homepage: www.elsevier.com/locate/biopha

DNA methylation-based depiction of the immune microenvironment and immune-associated long non-coding RNAs in oral cavity squamous cell carcinomas

Naiade Calanca [a,b,1], Ana Lucia Noronha Francisco [c,1], Daniela Bizinelli [d], Hellen Kuasne [e], Mateus Camargo Barros Filho [d], Bianca Campos Troncarelli Flores [a], Clóvis Antonio Lopes Pinto [f], Claudia Aparecida Rainho [b], Milena Botelho Pereira Soares [g,h], Fabio Albuquerque Marchi [i], Luiz Paulo Kowalski [c,i], Silvia Regina Rogatto [a,*]

[a] Department of Clinical Genetics, University Hospital of Southern Denmark-Vejle, Institute of Regional Health Research, University of Southern Denmark, Odense 5000, Denmark
[b] Department of Chemical and Biological Sciences, Institute of Biosciences, São Paulo State University (UNESP), Botucatu 18618-689, SP, Brazil
[c] Department of Head and Neck Surgery and Otorhinolaryngology, A.C.Camargo Cancer Center, São Paulo 01509-001, SP, Brazil
[d] International Research Center (CIPE), A.C.Camargo Cancer Center, São Paulo 01508-010, SP, Brazil
[e] Rosalind and Morris Goodman Cancer Institute, McGill University, Montreal H3A1A3, QC, Canada
[f] Department of Pathology, A.C.Camargo Cancer Center, São Paulo 01509-010, SP, Brazil
[g] Health Technology Institute, SENAI CIMATEC, Salvador 41650-010, BA, Brazil
[h] Gonçalo Moniz Institute, FIOCRUZ, Salvador 40296-710, BA, Brazil
[i] Department of Head and Neck Surgery, University of São Paulo Medical School, São Paulo 05402-000, SP, Brazil

ARTICLE INFO

Keywords:
Oral cancer
Tumor immune microenvironment
LncRNAs
DNA methylation
Deconvolution

ABSTRACT

Oral cavity squamous cell carcinoma (OSCC) is a complex and dynamic disease characterized by clinicopathological and molecular heterogeneity. Spatial and temporal heterogeneity of cell subpopulations has been associated with cancer progression and implicated in the prognosis and therapy response. Emerging evidence indicates that aberrant epigenetic profiles in OSCC may foster an immunosuppressive tumor microenvironment by modulating the expression of immune-related long non-coding RNAs (lncRNAs). DNA methylation analysis was performed in 46 matched OSCC and normal adjacent tissue samples using a genome-wide platform (Infinium HumanMethylation450 BeadChip). Reference-based computational deconvolution (MethylCIBERSORT) was applied to infer the immune cell composition of the bulk samples. The expression levels of genes encoding

Abbreviations: ARG1, arginase; BMIQ, beta-mixture quantile normalization; BS, bisulfite; ChAMP, Chip Analysis Methylation Pipeline; CTL, cytotoxic T-lymphocyte; DC, dendritic cell; DMPs, differentially methylated probes; EZH2, enhancer of zeste 2 polycomb repressive complex 2 subunit; FOXP3, forkhead box P3; GEO, Gene Expression Omnibus; GZMA, granzyme A; GZMB, granzyme B; H19, H19 imprinted maternally expressed transcript; HIF1A, hypoxia inducible factor 1 subunit alpha; HNSC, head and neck squamous cell carcinoma; HOTAIR, HOX transcription antisense RNA; HPV, human papillomavirus; HULC, hepatocellular carcinoma up-regulated long non-coding RNA; IDO1, indoleamine 2,3-dioxygenase 1; IFNG, interferon gamma; IL10, interleukin 10; IL12, interleukin 12; IL1B, interleukin 1 beta; IL2, interleukin 2; IL2RA, interleukin 2 receptor subunit alpha; IL6, interleukins 6; KLRK1, killer cell lectin like receptor K1; lncRNAKB, Long non-coding RNA Knowledgebase; lncRNAs, long non-coding RNAs; MALAT1, metastasis associated lung adenocarcinoma transcript 1; MDSCs, myeloid-derived suppressor cells; MEG3, maternally expressed 3; MIR155HG, MIR155 host gene; NK, natural killer; NOS2, nitric oxide synthase 2; OSCC, Oral squamous cell carcinoma; PCR, polymerase chain reaction; PDCD1, programmed cell death 1; PD-L1, programmed death-ligand 1; PRF1, perforin 1; PTGS2, prostaglandin-endoperoxide synthase 2; PTPRC, protein tyrosine phosphatase receptor type C; RNA-seq, RNA sequencing; RORC, RAR related orphan receptor C; RORγt, retinoid acid receptor-related orphan receptor gamma t; SMAD2, SMAD family member 2; STAT3, signal transducer and activator of transcription 3; TAMs, tumor-associated macrophages; TANs, tumor-associated neutrophils; TCGA, The Cancer Genome Atlas; TDO2, tryptophan 2,3-dioxygenase; TGFB1, transforming growth factor beta 1; TGFB2, transforming growth factor beta 2; TGFBR1, transforming growth factor beta receptor 1; TME, tumor microenvironment; TNF, tumor necrosis factor; TNM, Tumor Node Metastasis; Tregs, regulatory T-lymphocytes; Trp, tryptophan; WFDC21P, WAP four-disulfide core domain 21, pseudogene.

* Correspondence to: Department of Clinical Genetics, University Hospital, Vejle Institute of Regional Health Research, University of Southern Denmark, Beriderbakken 4, Vejle 7100, Denmark.
E-mail address: silvia.regina.rogatto@rsyd.dk (S.R. Rogatto).
[1] These authors contributed equally.

https://doi.org/10.1016/j.biopha.2023.115559
Received 15 June 2023; Received in revised form 18 September 2023; Accepted 19 September 2023
Available online 22 September 2023

immune markers and differentially methylated lncRNAs were investigated using The Cancer Genome Atlas dataset. OSCC specimens presented distinct immune cell composition, including the enrichment of monocyte lineage cells, natural killer cells, cytotoxic T-lymphocytes, regulatory T-lymphocytes, and neutrophils. In contrast, B-lymphocytes, effector T-lymphocytes, and fibroblasts were diminished in tumor samples. The hypomethylation of three immune-associated lncRNAs (*MEG3*, *MIR155HG*, and *WFDC21P*) at individual CpG sites was confirmed by bisulfite-pyrosequencing. Also, the upregulation of a set of immune markers (*FOXP3*, *GZMB*, *IL10*, *IL2RA*, *TGFB*, *IFNG*, *TDO2*, *IDO1*, and *HIF1A*) was detected. The immune cell composition, immune markers alteration, and dysregulation of immune-associated lncRNAs reinforce the impact of the immune microenvironment in OSCC. These concurrent factors contribute to tumor heterogeneity, suggesting that epi-immunotherapy could be an efficient alternative to treat OSCC.

1. Introduction

Oral cavity squamous cell carcinoma (OSCC) is a common tumor subtype that arises from the mucosal epithelium of oral cavity areas, including the anterior tongue, floor of the mouth, hard palate, and gingiva [1]. OSCC represents approximately 80–90% of all cases of oral cancer, accounting for more than half of head and neck squamous cell carcinomas (HNSC). It is estimated that the 2-year survival rate corresponds to 50% for HNSC at stages III and IV. Tobacco smoking and alcohol consumption have been identified as major risk factors [2]. Approximately 2% of all oral cavity cancers are attributable to human papillomavirus (HPV), and it is well-known that infected individuals have better responses to chemotherapy alone or along with radiotherapy [3]. Surgical resection followed by adjuvant therapy has been the typical treatment strategy in oral cancers if resectable, while unresectable tumors are generally submitted to palliative treatment with systemic therapy and/or radiotherapy [1,4].

Mounting evidence highlights the potential of harnessing immune response to treat patients with recurrent and metastatic disease and unresectable HNSC as the primary approach [5]. An immunosuppressive tumor microenvironment (TME) epigenetically modulates the gene expression program of immune cells and can promote tumor escape [6]. A meta-analysis study in HNSC showed that a high level of tumor-associated macrophages (TAMs) was related to a poor overall survival rate, primarily due to the secretion of immunosuppressive factors [7]. A recent study showcased the involvement of tumor-infiltrating immune cells during OSCC progression: cell populations with anti-tumor roles, such as CD8 + T-lymphocytes, tended to diminish, while those with pro-tumorigenic activity, such as myeloid-derived suppressor cells (MDSCs), exhibited enrichment in advanced-stage compared to early-stage disease [8]. Tumors can be classified into immune hot or cold according to their T cell infiltration patterns. Hot tumors are characterized by enriched cytotoxic T-lymphocyte (CTL) infiltration and better response to immune checkpoint inhibitors, while cold tumors are poorly infiltrated and usually fail to respond to checkpoint blockade [9]. Elucidating how tumors modulate an immunosuppressive TME is paramount to reprogramming the immunologic microenvironment towards an anti-tumor state and developing more efficient treatment strategies.

The characterization of the OSCC microenvironment has been largely based on RNA sequencing (RNA-seq) data. Three recent studies utilized CIBERSORT and/or ESTIMATE algorithms to analyze OSCC gene expression profiles and determine immune cell abundance and immune infiltration scores, respectively [10–12]. Zhang et al. [11] assigned OSCC patients to high- or low-risk groups according to the expression levels of shelterin complex genes, and the low-risk group showed higher immune scores and better prognosis [11]. Zhao et al. [12] highlighted that a higher immune score was associated with better prognosis in OSCC patients [12]. The cells recruited to the TME are known to be epigenetically modulated by microenvironment factors, including cytokines, chemokines, and growth factors [13]. Such epigenetic reprogramming includes changes in DNA methylation, histone modification, and chromatin structure. Previous evidence suggests that histone methyltransferase and DNA methyltransferase inhibitors may condition tumors from poor to rich T-cell infiltration [6]. Immune cell deconvolution of bulk DNA methylation data is a powerful tool to determine the proportion of different cell types in the TME [14]. This approach allows inferring the contribution of each cell population to the aberrantly methylated genes detected in bulk tissue specimens. Some of these differentially methylated genes promote reprogramming besides being epigenetically regulated. Long non-coding RNAs (lncRNAs), for example, can control the DNA methylation of other genes and serve as predictive and prognostic markers by presenting specific methylation patterns in cancer [15]. These transcripts spanning 200 nucleotides or more are not usually translated into proteins and have been implicated in regulating cellular processes at transcriptional, post-transcriptional, and epigenetic levels [16]. LncRNAs can also coordinate the expression of cytokine and other elements of immune cells [17]. In short, lncRNAs are promising candidate biomarkers for immune-mediated diseases and potential targets for cutting-edge therapeutic strategies [16].

Herein, we aimed to characterize the TME immune components from a cohort of OSCC, cross validating our findings with a larger cohort from The Cancer Genome Atlas (TCGA) HNSC project. We used an in-silico deconvolution approach to sort out the main immune cell populations infiltrating bulk OSCC specimens based on the DNA methylation analysis. Afterward, the transcriptome data from TCGA OSCC samples was assessed to evaluate the expression levels of genes encoding immune markers and immune-associated lncRNAs. This information allowed us to depict further the role of different immune cells in OSCC TME and to identify potential lncRNAs able to modulate the anti-tumor response. Once these lncRNAs were differentially methylated in both cohorts, our findings paved the way for a better understanding of how the immunologic TME is regulated in OSCC and how these regulatory mechanisms can be subverted for therapeutic purposes.

2. Material and methods

2.1. Patients

A cohort of 64 OSCC samples was retrospectively collected from patients who underwent surgery as the initial treatment at A.C. Camargo Cancer Center, São Paulo, Brazil, between 2006 and 2013. Patients with tumors resected with close or positive margins or metastatic lymph nodes with extracapsular spread underwent postoperative radiotherapy associated with platin-based chemotherapy. Patients with tumors at clinical stages III or IV or with primary tumors with vascular embolization, perineural infiltration, or metastatic lymph nodes without extracapsular spread underwent postoperative radiotherapy. Forty-six OSCC matched with normal adjacent tissue samples (discovery set) were evaluated by genome-wide DNA methylation analysis. Eighteen OSCC and eight adjacent normal tissues were included in the validation set. The study was approved by the institutional Ethics Committee (Protocol # 1876/14). All patients provided written informed consent before the sample collection. Clinical, histopathological, and therapeutic data were obtained from the medical records, and the follow-up was updated in August 2022.

The patients of the discovery set were diagnosed at the mean age of

56.7 ± 13.5 years, 72% were male, and the tongue was the main anatomic site affected by cancer (69.6%). The HPV genotyping was performed using the Linear Array HPV Genotyping Test (Roche Molecular Diagnostics, Branchburg, NJ, USA). Most cases were smokers (70%), alcohol consumers (85%), and HPV negative (70%) (Table 1).

A flowchart summarizing the study design and the analyses used to identify tumor-infiltrating immune cells and altered immune-associated lncRNAs in OSCCs is depicted in Fig. 1.

Table 1
Clinical and histopathological findings of OSCC patients included in this study.

Characteristics	Discovery set N = 46 (%)	Validation set N = 18 (%)
Age		
Mean ± SD	56.7 ± 13.5	60.5 ± 15.2
Gender		
Female	13 (28.3)	3 (16.7)
Male	33 (71.7)	15 (83.3)
Tumor site		
Tongue	32 (69.6)	7 (38.9)
Floor of mouth	4 (8.7)	3 (16.7)
Palate	4 (8.7)	1 (5.6)
Gingiva	5 (10.9)	6 (33.3)
Buccal mucosa	1 (2.2)	1 (5.6)
cT stage		
T1	1 (2.2)	2 (11.1)
T2	18 (39.1)	7 (38.9)
T3	14 (30.4)	4 (22.2)
T4	13 (28.3)	5 (27.8)
cN stage		
N0	19 (41.3)	10 (55.6)
N1	8 (17.4)	3 (16.7)
N2	18 (39.1)	5 (27.8)
N3	1 (2.2)	–
cM stage		
M0	45 (97.8)	18 (100)
M1	1 (2.2)	–
Tumor stage		
I	1 (2.2)	2 (11.1)
II	15 (32.6)	5 (27.8)
III	9 (19.6)	6 (33.3)
IV	19 (41.3)	5 (27.8)
NA	2 (4.3)	–
HPV status[†]		
Positive	14 (30.4)	–
Negative	32 (69.6)	–
Tobacco Smoking		
Yes	32 (69.6)	13 (72.2)
No	14 (30.4)	5 (27.8)
Alcohol Consumption		
Yes	39 (84.8)	13 (72.2)
No	7 (15.2)	5 (27.8)
Postoperative radiotherapy		
Yes	40 (87.0)	14 (77.8)
No	6 (13.0)	4 (22.2)
Postoperative chemotherapy		
Yes	21 (45.7)	5 (27.8)
No	25 (54.3)	13 (72.2)
Vital status		
Alive	26 (56.5)	10 (55.6)
Deceased	17 (37.0)	7 (38.9)
NA	3 (6.5)	1 (5.6)
Local recurrence		
Yes	9 (19.6)	2 (11.1)
No	35 (76.1)	16 (88.9)
NA	2 (4.3)	–
Second primary tumor		
Yes	3 (6.5)	2 (11.1)
No	43 (93.5)	16 (88.9)
Distant metastasis		
Yes	8 (17.4)	2 (11.1)
No	36 (78.3)	16 (88.9)
NA	2 (4.3)	–
Follow-up: median months	62.4 (IQR = 86.3)	57.8 (IQR = 46.4)

SD: standard deviation; NA: information not available; IQR: interquartile range.
[†] All the positive cases were infected by HPV 16.

2.2. DNA methylation data analysis

Genome-wide DNA methylation analysis was performed using the Infinium Human Methylation450 BeadChip (Illumina, San Diego, CA, USA). DNA methylation data, described as beta values of continuous variables between 0 and 1, were recorded for each locus in each sample. The quality control parameters were followed, and probes were filtered, normalized, and adjusted using the R Bioconductor package Chip Analysis Methylation Pipeline (ChAMP) (v.2.24.0) [18,19]. Briefly, cross-reactive probes (≥49 bases), single nucleotide polymorphisms (Minor Allele Frequency >5%), gender-associated probes, low quality probes ($p > 0.05$), and low bead count (<3) in at least 5% of samples were removed. Data were normalized using the Beta-MIxture Quantile Normalization (BMIQ) method and the annotation was performed according to the Illumina manifest (hg19) and HUGO Gene Nomenclature Committee [20]. The sample groups were compared, and the differentially methylated probes (DMPs) were identified using the limma package (v.3.50.3) considering a Bonferroni-adjusted p-value < 0.05 and a mean delta-beta ($\Delta\beta$) ≥ 0.2 or ≤ -0.2 [21].

2.3. Cross-validation analysis using DNA methylation and transcriptomic data

A cross-study validation analysis was performed using genome-wide DNA methylation data of 344 OSCC samples and 34 adjacent normal samples from the TCGA-HNSC dataset [22]. The methylome data was retrieved using the UCSC Xena browser (https://xena.ucsc.edu/) [23]. DMPs were investigated using the same pipeline applied to analyze our internal dataset.

Transcriptomic data (RNA-seq) of 292 OSCC and 19 normal samples from the TCGA-HNSC dataset was downloaded with the R Bioconductor package TCGAbiolinks (v.2.25.2) [24,25]. The RNA-seq count data (Spliced Transcripts Alignment to a Reference method) was annotated with the biomaRt package (v.2.50.3) [26]. The Ensembl IDs that did not match Entrez Gene, Gene Symbol, or Gene Biotype were excluded. Next, a variance stabilizing transformation was performed following the DESeq2 package pipeline (v.1.34.0) [27]. The differences in the global gene expression between tumor and normal samples were calculated with the limma package (v.3.50.3) for a panel of immune markers and selected lncRNAs associated with immune cell populations [21].

2.4. Distribution of differentially methylated probes per region

The DMPs were classified into different groups in terms of their distributions relative to gene regions (TSS1500, TSS200, 5′UTR, first exon, gene body, 3′UTR, or intergenic region) and CpG island location (island, shore, shelf, or open sea) according to Infinium HumanMethylation450 BeadChip annotation. DMPs in TSS1500, TSS200, 5′UTR, and first exon regions were grouped into the promoter region category. The proportion of probes per region was calculated with the 21,085 probes remaining after filtering, normalization, and differential methylation analysis.

2.5. Reference-based deconvolution

Our methylation matrix composed of 46 paired OSCC and normal samples data and the ten cell type-signature matrix derived by Chakravarthy et al. were uploaded onto CIBERSORTx (https://cibersortx.stanford.edu/, last accessed in July 2022) [28]. The analysis was run in relative mode using 1000 permutations without quantile normalization. Similar procedures were used to investigate DNA methylation data from the TCGA cohort.

2.6. LncRNAs selection

DMPs annotated by gene symbols using Illumina manifest file were

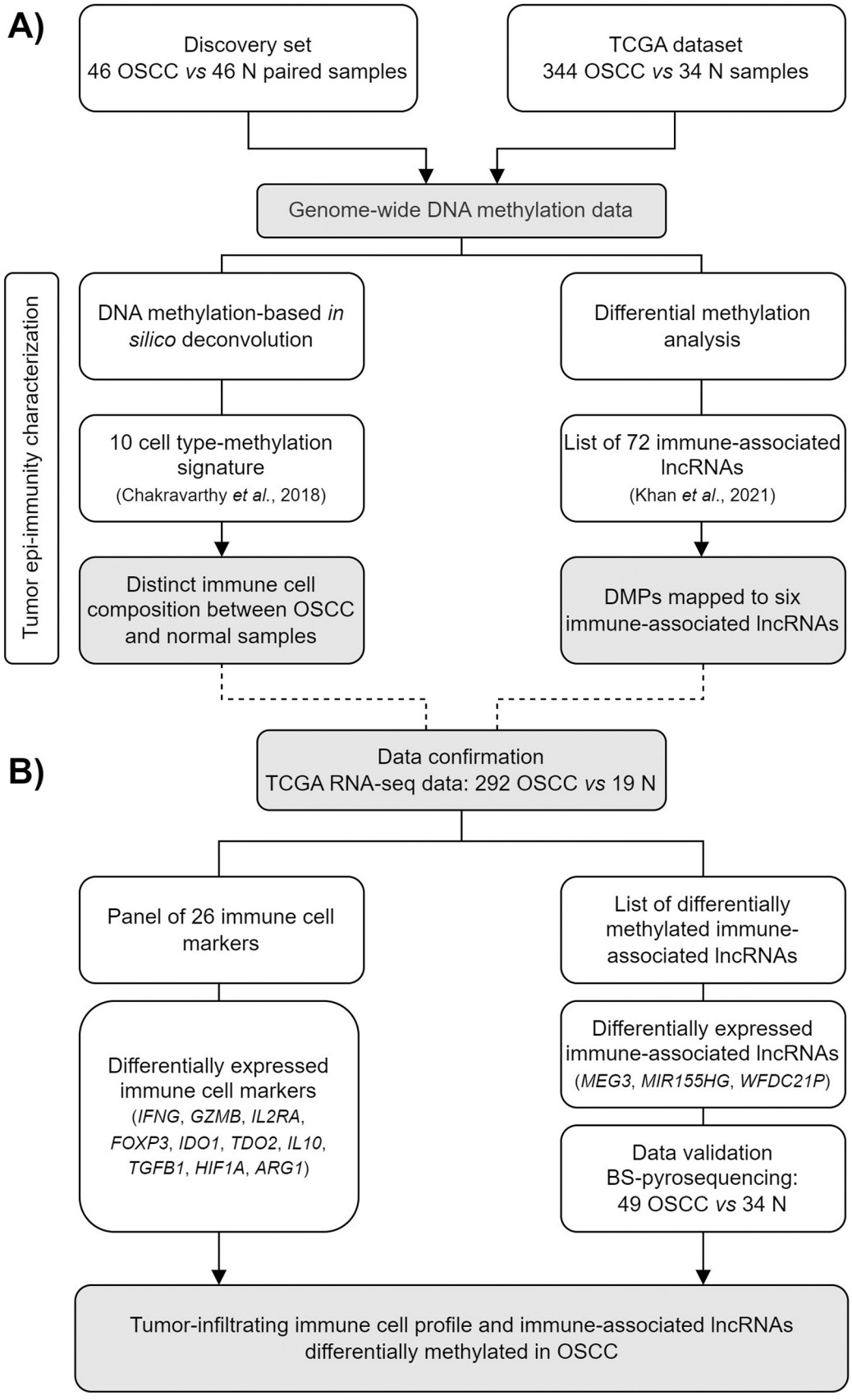

(caption on next page)

Fig. 1. Flowchart describing the methodology used to identify tumor-infiltrating immune cells and altered immune-associated lncRNAs in OSCC. **A)** Bulk DNA methylation data obtained from 46 matched OSCC and normal samples (discovery set) and the TCGA dataset (344 OSCC and 34 normal samples) was analyzed by two different approaches. *In silico* deconvolution was applied to infer the immune cell composition of the tumor microenvironment using ten cell types-reference derived from Chakravarthy et al. [28]. The second approach used differential methylation analysis that revealed DMPs common to both datasets. DMPs mapped to lncRNAs implicated in immune cell functions, as reported by Khan et al. [31], were selected for further analysis. **B)** The expression levels of genes encoding immune markers (26 genes) and differentially methylated lncRNAs were investigated using RNA-seq data of 292 OSCC and 19 normal samples from the TCGA dataset. Three immune-associated lncRNAs (*MEG3*, *MIR155HG*, and *WFDC21P*) were differentially expressed in the OSCCs samples from TCGA. The methylation status of these lncRNAs was validated at individual CpG sites by BS-pyrosequencing in 49 OSCC and 39 normal samples. These analyses allowed us to depict the immune cell infiltration in OSCC and identify altered lncRNAs that potentially modulate the anti-tumor response. OSCC: oral squamous cell carcinoma; N: normal samples; TCGA: The Cancer Genome Atlas; RNA-seq: RNA sequencing; lncRNAs: long non-coding RNAs; DMPs: differentially methylated probes; BS: bisulfite.

investigated to select those related to protein-coding genes and lncRNAs using biomaRt (v.2.50.3) and org.Hs.eg.db (v.3.14.0) packages, and long non-coding RNA Knowledgebase (lncRNAKB) (http://www.lncrnakb.org/, last accessed 16 Aug 2022) [26,29]. All probes ambiguously annotated were checked in the literature. Unsupervised k-means clustering was conducted to analyze the methylation patterns of protein-coding genes (N = 13,239) and lncRNAs (N = 263). The heatmaps were plotted using the ComplexHeatmap package (v.2.10.0) [30].

The 263 differentially methylated lncRNAs from our internal dataset were then compared to a list of 72 immune-related lncRNAs reported by Khan et al. [31]. A Pearson correlation analysis of RNA-seq and methylation data (R values with $p < 0.05$) for TCGA OSCC samples (N = 254) was performed. All probes for each immune-related lncRNA found in both datasets showed a significant difference in methylation between normal and cancer tissue samples ($p < 0.05$). Eight probes showing concordance with our internal dataset were observed for four lncRNAs (*HOTAIR*, *MEG3*, *MIR155HG*, and *WFDC21P*). The lncRNAs *WFDC21P* (also known as *lnc-DC*) (cg12320164), *MEG3* (cg08294662, cg09285543), and *MIR155HG* (cg13309012) were selected for further investigation (bisulfite-pyrosequencing). Although the dendritic cell (DC) population is not covered in our deconvolution analysis, the *lnc-DC* was selected due to the role of these cells in the cellular antitumor response.

2.7. Site-specific DNA methylation evaluated by bisulfite pyrosequencing

Bisulfite (BS)-pyrosequencing was used to assess the DNA methylation levels of four selected CpGs mapped to three lncRNAs in 49 OSCC (31 from the discovery set and 18 from the validation set) and 34 adjacent normal samples. Primer sequences and polymerase chain reaction (PCR) conditions used in the BS-pyrosequencing for each CpG site are described in Supplementary Table 1. After bisulfite conversion, 30 ng of DNA were amplified using the PyroMark PCR kit (Qiagen, Redwood, CA, USA), according to the manufacturer's protocol. The PCR products were sequenced on the PyroMark Q24 system (Qiagen).

2.8. Expression profile of immune markers in the TCGA-OSCC dataset

We selected 26 immune markers whose expression levels could impact the function of the immune cell populations. This selection was based on the literature data and the relevance of these cell populations (enriched or diminished in OSCC compared to normal samples) in the deconvolution analysis. RNA-seq data of 292 TCGA-OSCC and 19 normal samples were analyzed to evaluate the differences in the gene expression levels of these 26 immune cell markers: *CD4*, *CD8A*, *CD8B*, protein tyrosine phosphatase receptor type C (*PTPRC*), interferon gamma (*IFNG*), granzyme A (*GZMA*), granzyme B (*GZMB*), perforin 1 (*PRF1*), interleukin 2 receptor subunit alpha (*IL2RA*), forkhead box P3 (*FOXP3*), indoleamine 2,3-dioxygenase 1 (*IDO1*), tryptophan 2,3-dioxygenase (*TDO2*), interleukins 6 (*IL6*), 10 (*IL10*), and 1 beta (*IL1B*), tumor necrosis factor (*TNF*), transforming growth factor beta 1 (*TGFB1*), programmed cell death 1 (*PDCD1*), *CD274* (or PD-L1 - programmed death-ligand 1), arginase 1 (*ARG1*), prostaglandin-endoperoxide synthase 2 (*PTGS2*), killer cell lectin like receptor K1 (*KLRK1*), nitric oxide synthase 2 (*NOS2*), signal transducer and activator of transcription 3 (*STAT3*), and hypoxia inducible factor 1 subunit alpha (*HIF1A*).

2.9. Statistical analysis

Statistical analyses and graphical representations were performed using Prism 9.0 (GraphPad Software Inc., San Diego, CA, USA) and R software v.4.2.1 (https://www.r-project.org/). Non-parametric t (Mann-Whitney) test was used for all analyses comparing normal versus tumor samples or immune hot versus immune cold groups. The correlation between the cell fractions estimated by CIBERSORTx and clinicopathological information was evaluated in the discovery set using simple logistic regression. Log-rank (Mantel–Cox) test was used for survival analysis. The score cutoffs for survival-associated immune cell populations were calculated with the easyROC web tool (v.1.3.1) [32]. The null hypothesis was rejected when the two-tailed p-value was < 0.05.

3. Results

3.1. DNA methylation profile

The DNA methylation profile of 46 OSCC samples of the internal dataset was compared to normal samples and the data generated is available in the Gene Expression Omnibus (GEO) database (GSE234379, https://www.ncbi.nlm.nih.gov/geo/).

We found 21,085 DMPs (13,342 hypo- and 7743 hypermethylated probes), most of them (63%) hypomethylated. Unsupervised clustering analysis using DMPs mapped to lncRNAs and protein-coding genes showed two groups comprising normal and tumor samples, except for one normal sample (Fig. 2A and B). In parallel, the TCGA-OSCC dataset analysis resulted in 39,245 DMPs (19,932 hypo- and 19,313 hypermethylated probes). A total of 16,500 DMPs (37.6%) from our dataset presented methylation patterns similar to those from TCGA-OSCC samples, including 9816 hypomethylated and 6684 hypermethylated CpGs (Fig. 2C).

An enrichment of hypermethylated CpGs was detected in gene promoters, whereas hypomethylated CpGs were mainly located in intergenic regions (Fig. 2D). Hypermethylated CpGs were frequently detected in CpG islands (47.72%), while hypomethylated were predominantly located in open sea regions (70.20%) (Fig. 2E).

3.2. DNA methylation-based deconvolution reveals distinct immune cell populations in OSCC

DNA methylation data from internal and TCGA datasets were explored using digital cytometry to characterize the immune cell populations in OSCC (Fig. 3). Tumor samples from the internal dataset presented a significantly increased proportion of monocyte lineage cells (monocytes, macrophages, MDSCs), natural killer (NK) cells, CTLs, neutrophils, and regulatory T-lymphocytes (Tregs). A significantly decreased proportion of B-lymphocytes, effector T-lymphocytes, eosinophils, and fibroblasts was detected in tumor samples compared to normal specimens. Similarly, the scores derived from the TCGA cases revealed that the monocyte lineage cells, NK cells, and neutrophils were significantly enhanced in tumors, while the composition of B-

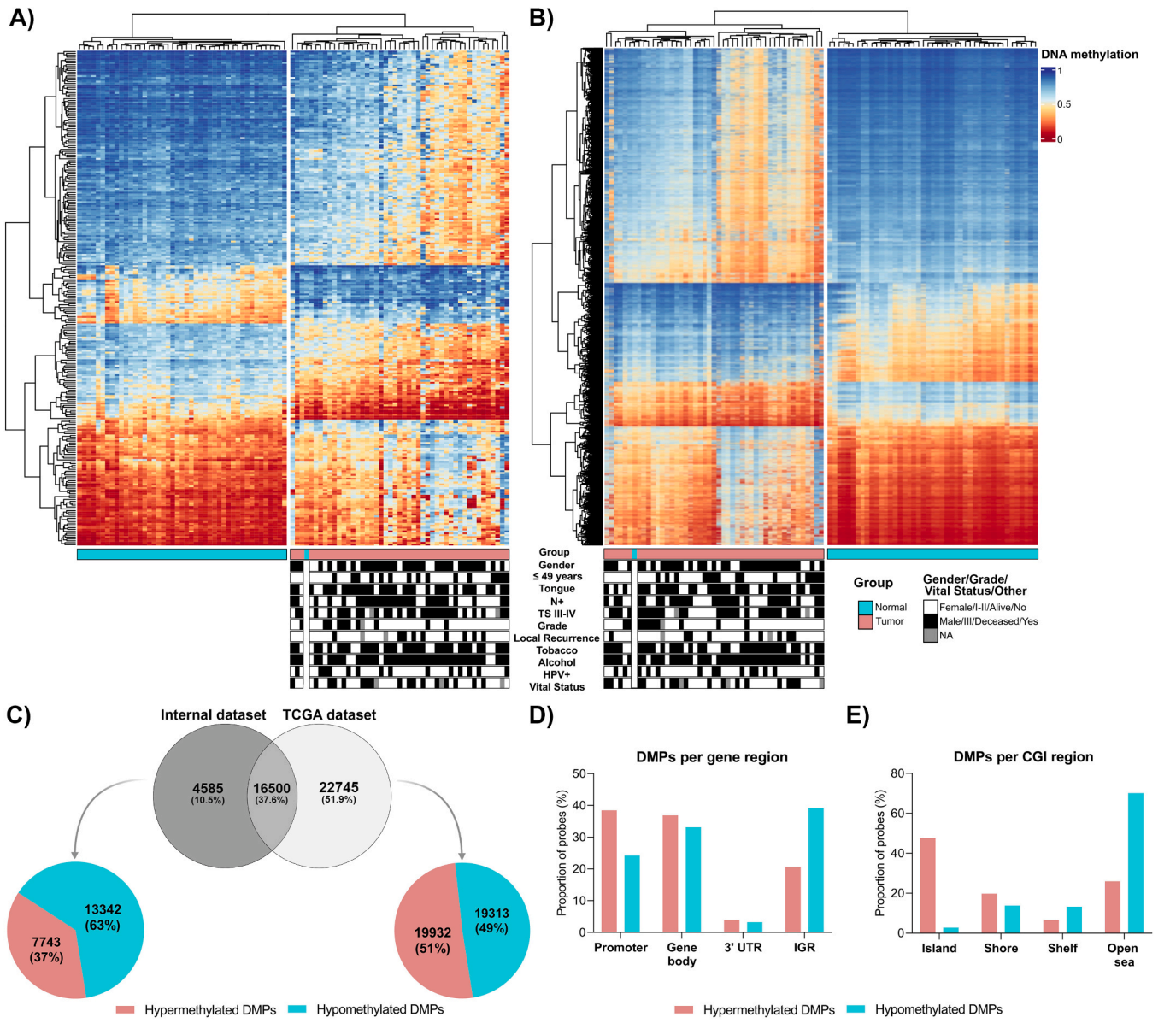

Fig. 2. Differentially methylated probes (DMPs) in oral squamous cell carcinomas (OSCC). The heatmaps depict the DNA methylation profile of differentially methylated **(A)** lncRNAs and **(B)** protein-coding genes in samples from the internal cohort considering Bonferroni-adjusted p-value < 0.05 and $\Delta\beta \geq 0.2$ or ≤ -0.2. The clustering analysis was performed using the k-means algorithm (K = 2). **C)** Comparison between DMPs identified in the internal and TCGA-OSCC datasets and proportion of hypo- and hypermethylated probes detected in each project. The histograms show the relative frequency distribution of DMPs according to **(D)** gene region and **(E)** CpG island (CGI) region in our internal OSCC samples. Illumina's field guide to methylation methods defines CGIs as regions with length > 500 bp, GC content > 55% and expected/observed CpG ratio of > 0.65, CpG shores as 0–2 kb from islands and CpG shelves as 2–4 kb from islands. Open sea consists of regions not located in any regions relating to CGIs. The hypermethylated DMPs are represented in pink, and the hypomethylated DMPs in green.

lymphocytes and fibroblasts was also distinct in normal samples. Interestingly, although not significant, the TCGA-OSCC samples presented a trend to decreased proportions of effector T-lymphocytes and increased Tregs infiltration, as observed in the internal dataset (Fig. 3).

Among the tumor samples from the internal cohort, we derived two immune clusters by performing unsupervised hierarchical clustering on the cell fractions estimated by CIBERSORTx. The two clusters showed distinct infiltrating cell types: B-lymphocytes, NK cells, CTLs, eosinophils, and neutrophils (Fig. 4A and B). Eight OSCC cases displaying significantly higher B-lymphocytes, CTLs, and eosinophils proportion and higher average scores (the average score of nine cell types calculated for each sample) were classified as immune hot tumors. However, no significant survival benefits for patients included in any of the clusters were observed (Fig. 4C). Once we detected an increased proportion of the abovementioned cell types, we also investigated their association with overall survival. The calculated score cutoffs for B-lymphocytes, CTLs, and eosinophils were 0.06548577, 0.1211135, and zero, respectively. Values above these cutoffs were defined as high. We found a marginal significance in patients with higher B-lymphocyte scores (N = 17) and longer overall survival ($p = 0.0584$; log-rank test) (Fig. 4C).

3.3. Cellular infiltration patterns according to clinical information

The infiltration patterns of 10 cell populations of our OSCC cohort showed no statistical difference when comparing HPV-positive and -negative tumors (Supplementary Figure 1). A similar comparison with the TCGA cohort revealed that HPV-positive tumors exhibited increased proportions of neutrophils and fibroblasts. The HPV-negative specimens presented enhanced monocyte lineage cells infiltration and a trend to

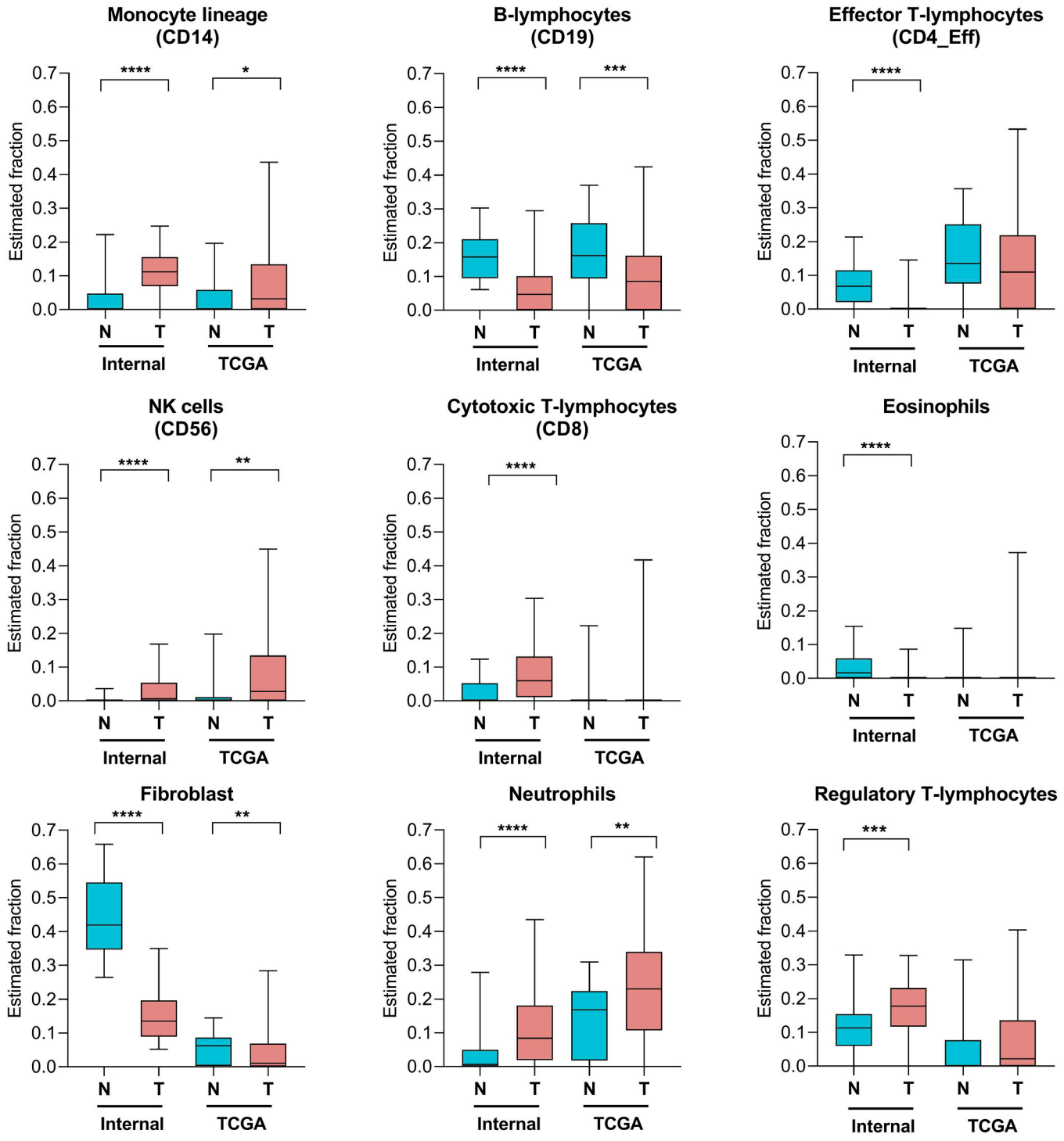

Fig. 3. Immune profile characterization of oral squamous cell carcinoma (OSCC) samples using the CIBERSORTx deconvolution analysis. Boxplots of estimated fractions of nine cell types for OSCC and normal samples from the internal and external cohorts by sample status. The statistical difference was determined with the Mann–Whitney test. * $p \leq 0.05$, ** $p \leq 0.01$, *** $p \leq 0.001$, **** $p \leq 0.0001$. The boxplots' edges and middle lines represent the lower and upper quartiles and the medians, respectively. The whiskers extend from the minimum to the maximum value.

increased infiltration of Tregs.

The immune cell infiltration pattern and other clinicopathological variables of our dataset were compared using association analysis (Fig. 4, Supplementary Figure 2). Higher levels of NK cells were associated with lymph node metastasis, while reduced infiltration of fibroblasts and monocyte lineage cells was associated with alcohol consumption and young-OSCC onset (≤ 49 years), respectively. Additionally, considering the immune hot and cold clusters we derived in the previous subsection, higher B-cells levels and lower levels of neutrophils and NK cells were associated with the immune hot pattern (Fig. 5).

3.4. *Differentially methylated and expressed immune cell-associated lncRNAs*

To better characterize the immune infiltration in OSCC, we further investigated the DNA methylation status and expression of lncRNAs with

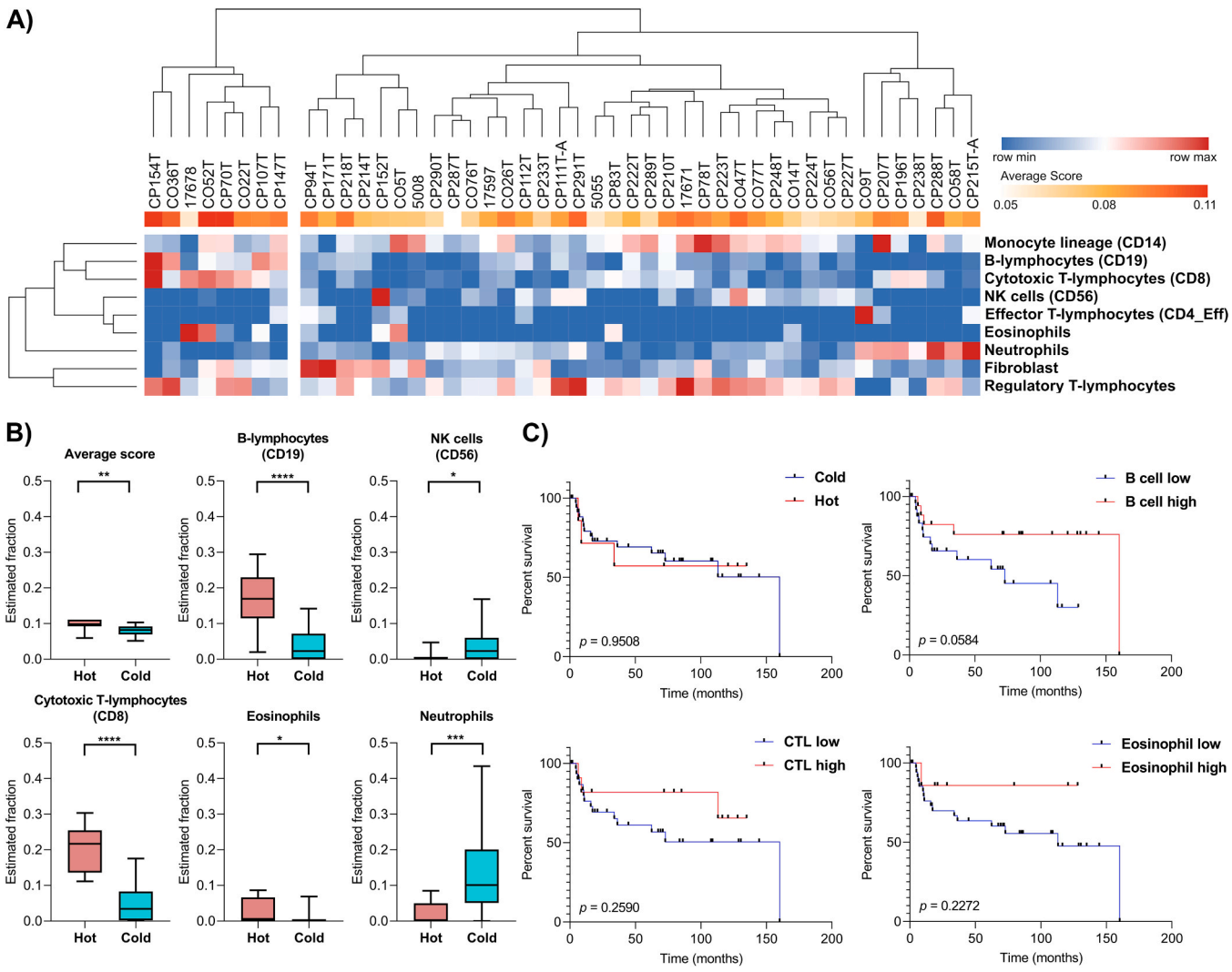

Fig. 4. Classification of oral squamous cell carcinoma (OSCC) samples as immune hot or cold. **A)** Heatmap representative of immune cells and fibroblast fractions of OSCC samples from the internal dataset using CIBERSORTx analysis. Rows and columns were clustered using the Euclidean distance of the estimated fraction values. The average score was calculated for each sample considering the estimated fraction of nine cell types. **B)** Boxplots of cell types based on the two clusters (referred to as hot and cold) derived from OSCC samples (Fig. 3A). The estimated fraction of each cell type in hot versus cold tumors was represented only for significant differences ($p < 0.05$, Mann-Whitney or unpaired t-test). * $p \leq 0.05$, ** $p \leq 0.01$, *** $p \leq 0.001$, **** $p \leq 0.0001$. **C)** Kaplan–Meier curves showing the impact of immune hot and cold clusters, B-lymphocytes, cytotoxic T-lymphocytes (CTLs), and eosinophils on survival of OSCC patients (*p*-values from Log-rank Test). The score cutoffs for survival analysis were determined with the easyROC web tool. The boxplots' edges and middle lines represent the lower and upper quartiles and the medians, respectively. The whiskers extend from the minimum to the maximum value.

experimentally demonstrated activities in immune cells. We analyzed the DNA methylation status of 72 immune cell-associated lncRNAs reported by Khan et al. [31] in 344 OSCC and 34 adjacent normal samples of the TCGA dataset. We compared the differentially methylated lncRNAs detected in the TCGA with our cohort and found six lncRNAs altered in both cohorts; four of them were also differentially expressed in the TCGA dataset (HOX transcription antisense RNA - *HOTAIR*, H19 imprinted maternally expressed transcript - *H19*, maternally expressed 3 - *MEG3*, and MIR155 host gene - *MIR155HG*) (Fig. 6A and B, Supplementary Figure 3).

Two lncRNAs (*MEG3* and *MIR155HG;* DMPs mapped in gene bodies) showing hypomethylation in tumor samples (internal and TCGA datasets) and presenting differential expression in the TCGA cohort (Fig. 6A and B) were evaluated by bisulfite (BS)-pyrosequencing. Pearson correlation analysis between the DNA methylation and gene expression levels was significantly positive for all the probes mapped to *HOTAIR* and *MEG3.* In contrast, the DMP mapped to the *MIR155HG* exhibited a negative correlation (Supplementary Figure 4). One DMP (cg12320164) located in the promoter region of the WAP four-disulfide core domain 21, pseudogene (*WFDC21P*, also known as *lnc-DC*), expressed explicitly in human DCs, was also selected for validation. *WFDC21P* was hypomethylated and downregulated in TCGA-OSCC samples. These findings are detailed in Fig. 6C.

3.5. DNA methylation status of immune-related lncRNAs in OSCC samples

BS-pyrosequencing was performed in two DMPs (cg08294662 and cg09285543) associated with *MEG3*, one (cg13309012) with *MIR155HG*, and one (cg12320164) with *WFDC21P* to confirm their DNA methylation status. We used adjacent normal and OSCC specimens from the validation set (18 cases) and 31 cases from the discovery set. By comparing the CpG methylation levels between tumor and normal samples, we observed that all three lncRNAs were hypomethylated in OSCC, as previously detected with the differential DNA methylation analysis performed in the internal and TCGA datasets (Fig. 6A-C).

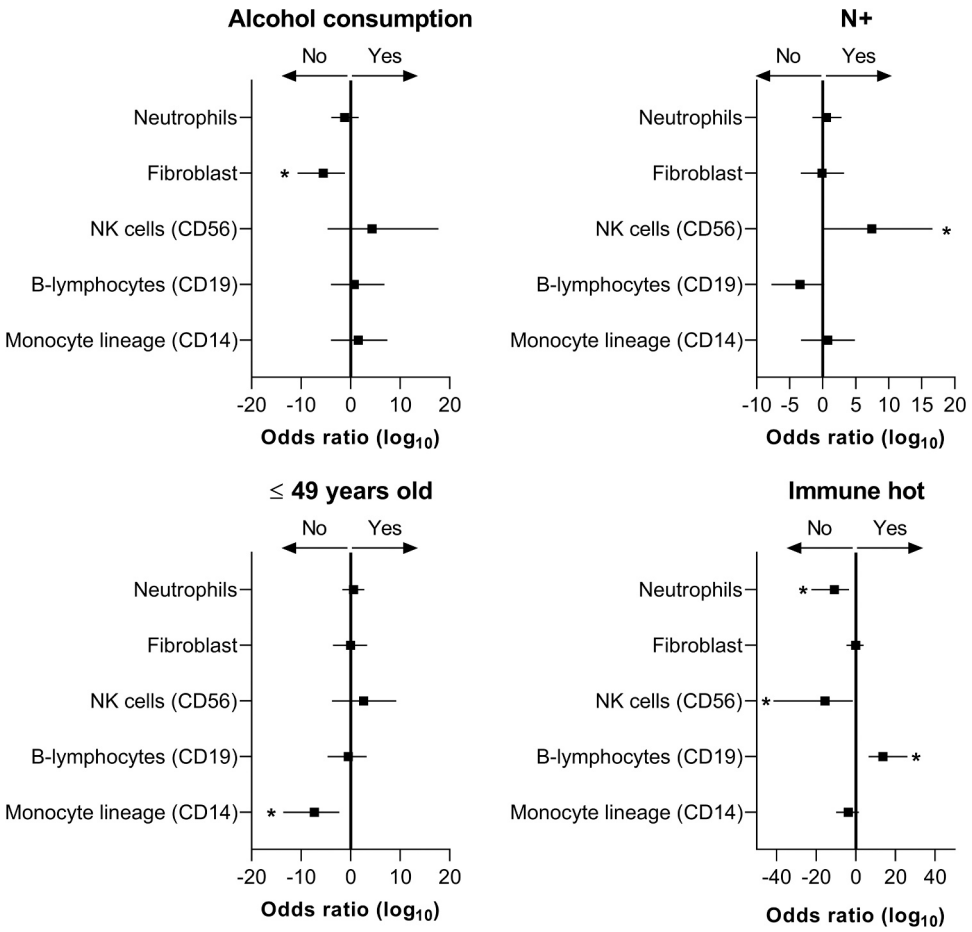

Fig. 5. Correlation analysis among estimated cell fractions and clinical variables of 46 oral squamous cell carcinoma (OSCC) patients from the discovery set. The forest plots show unadjusted Odds Ratios (with their 95% confidence intervals) of the absolute percentage of five cell populations compared to each clinicopathological variable (presence versus absence). Only cell populations showing significant differences between tumor and normal samples in internal and TCGA datasets were considered for this analysis. * $p \leq 0.05$.

3.6. mRNA expression of immune markers

The gene expression levels of 26 immune cell markers in 292 OSCC and 19 normal samples from TCGA revealed that tumor specimens displayed significant upregulation of *IFNG*, *GZMB*, *IL2RA*, *FOXP3*, *IDO1*, *TDO2*, *IL10*, *TGFB1*, and *HIF1A*, and downregulation of *ARG1* (Fig. 7). Albeit the difference was not statistically significant for the other markers, tumor samples presented trends to increased levels of *CD4*, *CD274*, *GZMA*, *PRF1*, *PTGS2*, *IL1B*, and *KLRK1*, and decreased levels of *CD8A*, *CD8B*, *PDCD1*, *TNF*, *IL6*, and *STAT3*.

Supplementary Figure 5 summarizes the main findings of the deconvolution using DNA methylation of our cohort of OSCC.

4. Discussion

Previous epigenetic studies in OSCC have demonstrated that altered DNA methylation is linked with cancer development and progression [33,34]. We found a distinct profile of DMPs associated with lncRNAs and protein-coding genes in tumor samples compared to paired normal adjacent oral mucosa, except for one normal sample. As expected for malignant cells, we detected an enrichment of hypermethylated DMPs in CpG islands and promoter regions [35]. Comparison between the global methylation profile of the internal discovery (46 OSCC) and TCGA (344 OSCC) cohorts revealed 37.6% of overlapping DMPs. A plausible explanation is that, unlike the internal cohort, OSCC and normal samples from the TCGA cohort are not paired. This is a limiting feature to the differential methylation analysis due to uncontrolled variables such as age, genetic background, and exposure to risk factors of different individuals. However, the DMPs common to both datasets showed the same methylation pattern (hyper- or hypomethylation), reinforcing their relevance to the disease.

To estimate the extent of the immune infiltration in OSCC samples, we determined the relative abundance of eight immune cell populations using the methylome data from internal and TCGA cohorts with MethylCIBERSORT [28]. We also assessed the correlation between the immune cell infiltration pattern and clinicopathological variables in OSCC samples from the discovery set. We detected increased tumor infiltrating CTLs in the internal cohort. When comparing tumor and normal samples from TCGA, there was no significant difference in *CD8A* and *CD8B* expression levels, genes encoding cell surface glycoproteins commonly found on these lymphocytes. The CTL effector genes *IFNG* and *GZMB* presented an increased expression. IFNγ is a cytokine that participates in multiple processes of antitumor immunity, including inhibition of tumor cells proliferation, activation of myeloid cells, antigen presentation, and maturation of CTLs, while granzyme B is a potent protease that rapidly induces target cell apoptosis [36,37]. IFNγ signaling in CD8 + T cells leads to the upregulation of granzyme [36]. NK cells can also produce these effector molecules and their infiltration was increased in OSCC from both internal and TCGA cohorts. Moreover, NK cells were modestly associated with lymph node metastasis in our OSCC samples ($p = 0.0437$). The reduced size of the internal cohort was a limitation in finding a strong association between tumor-infiltrating immune cells and clinical data. *IL2RA* is expressed in activated NK cells and promotes their affinity for IL-2 (interleukin 2), driving T cell proliferation and the

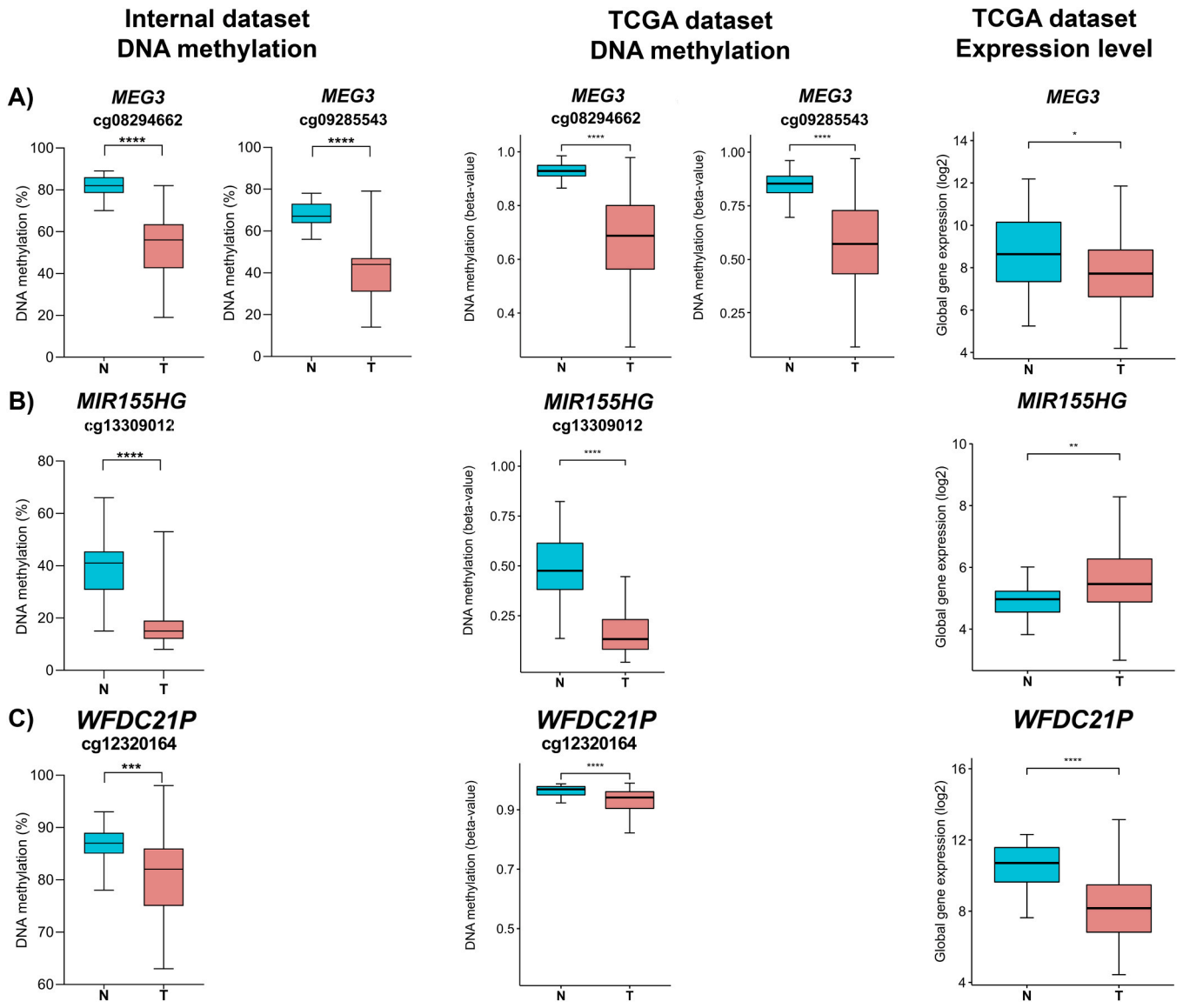

Fig. 6. DNA methylation and expression profile of immune-related lncRNAs in oral squamous cell carcinomas (OSCC). The boxplots on the left panel show the DNA methylation levels of differentially methylated probes (DMPs) mapped to lncRNAs *MEG3* **(A)**, *MIR155HG* **(B)**, and *WFDC21P* (also known as *lnc-DC*) **(C)** validated by BS-pyrosequencing (discovery and validation sets). The boxplots on the middle and right panels represent the DNA methylation (beta-value) and expression (log2) levels of the same lncRNAs in OSCC compared to normal samples retrieved from TCGA cohort. The statistical difference was determined with the Mann–Whitney test. * $p \leq 0.05$, ** $p \leq 0.01$, *** $p \leq 0.001$, **** $p \leq 0.0001$. The boxplots' edges and middle lines represent the lower and upper quartiles and the medians, respectively. The whiskers extend from the minimum to the maximum value.

production of cytolytic molecules, such as granzyme B [38]. The *IL2RA* expression was enhanced in TCGA-OSCC cohort.

A set of tumor samples showed increased CTLs and B-lymphocyte proportions, as well as a higher average score of immune cells and fibroblasts, i.e., immune hot phenotype. Chakravarthy et al., who developed MethylCIBERSORT, used this deconvolution pipeline for the first time to evaluate the tumor composition of TCGA pan-cancer, including HNSC samples [28]. Consistently with our results, they found that HNSC hot and cold tumors presented significant differences in the distribution of CTLs, B-cells, NK cells, and neutrophils. Herein, we used the publicly available methylation signature generated by these authors focusing exclusively on OSCC cases. CTLs possess antitumoral activity through recognition and lysis of tumor cells; therefore, they have antitumoral activity and are related to a favorable prognosis [7]. The high prevalence of CTLs has been correlated with improved survival in OSCC [39,40]. In our internal cohort, higher CTL scores and immune hot context did not provide statistically significant survival benefits possibly due the small sample size evaluated. However, patients with higher B-lymphocyte scores tended to present better survival. Previously, Lao et al. [41] reported a positive correlation between the density of CD19 + stroma-infiltrating B cells and overall survival in tongue squamous cell carcinomas [41]. B-lymphocytes, which can secrete cytokines such as IL-2 and act as antigen presenting cells, are key components of the TME, and most subtypes of tumor-infiltrating B cells, except for regulatory B cells, have been associated with favorable prognoses for different cancer types, including HNSC [42,43].

We also found an enrichment of Tregs in our OSCC samples. Tregs have immunosuppressive effects and can inhibit the CTLs functions [7]. The expression levels of *FOXP3*, which is a marker of Tregs and determines their fate, were enhanced among the TCGA-OSCC samples. This finding agrees with previous results from whole blood of HNSC patients showing augmented *FOXP3* expression [44]. Recent studies reported that besides modulating the differentiation and function of Tregs, *FOXP3* is expressed in various cancer types [45]. Additionally,

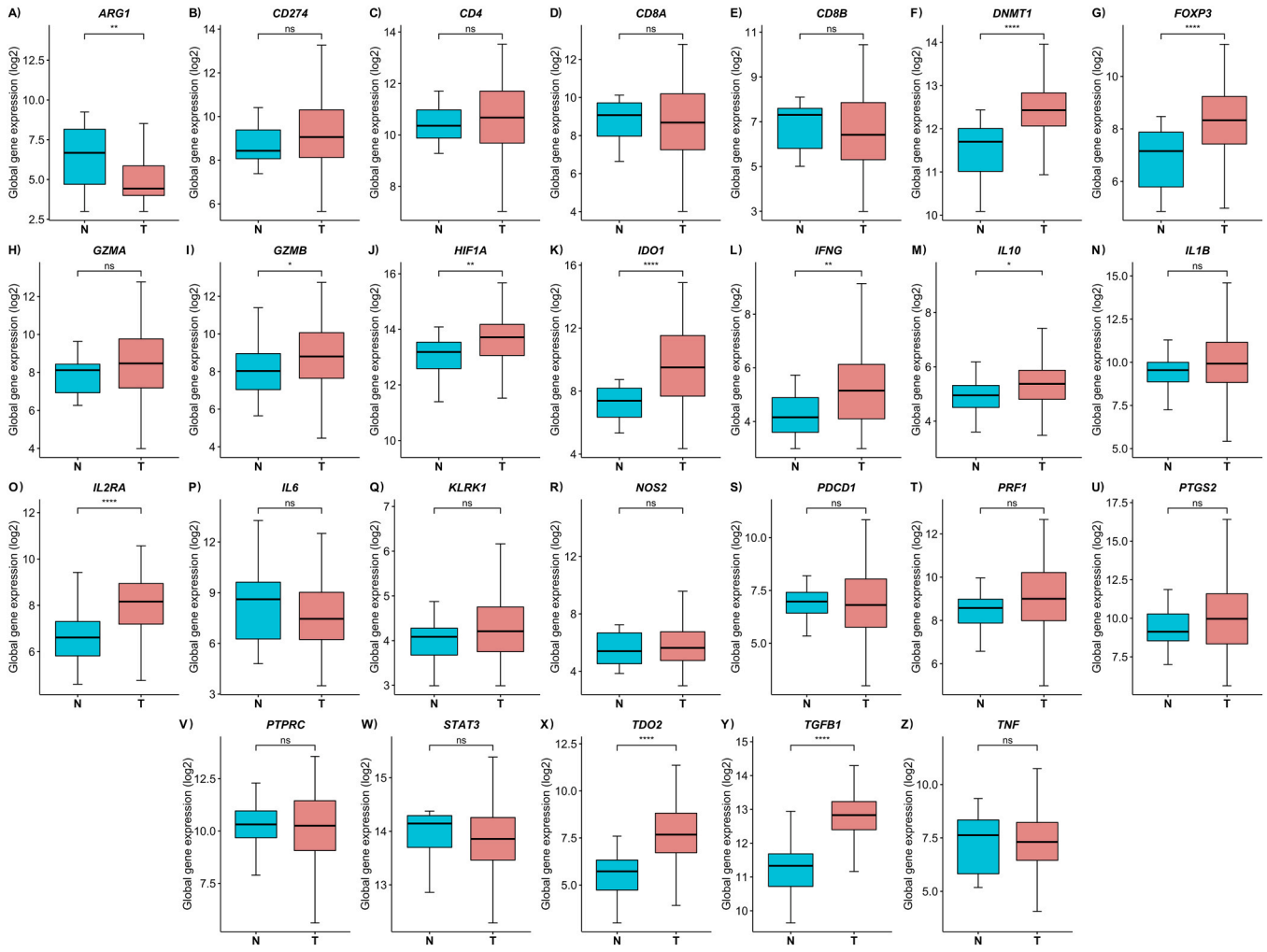

Fig. 7. Expression profile of immune cell markers in oral squamous cell carcinomas (OSCC) from TCGA. A-Z) Boxplots representative of expression levels (log2) of genes encoding immune markers in OSCC compared to normal samples from the TCGA cohort. The statistical difference was determined with the Mann–Whitney test. ns: not significant, * $p \leq 0.05$, ** $p \leq 0.01$, *** $p \leq 0.001$, **** $p \leq 0.0001$. The boxplots' edges and middle lines represent the lower and upper quartiles and the medians, respectively. The whiskers extend from the minimum to the maximum value.

cancer cells can express two other factors with immunosuppressive effects, IDO1 and TDO2, which are enzymes involved in the catabolism of amino acid tryptophan (Trp) [46]. These molecules were shown to be upregulated in OSCC samples. *IDO1* can either be expressed constitutively or induced by tumor-infiltrating immune cells that secrete inflammatory cytokines, such as IFNγ [46]. Through Trp depletion and generation of Trp catabolites, IDO1 induces Tregs and MDSCs and suppresses the proliferation and function of effector T and NK cells [46,47]. TDO2 has been shown to favor a pro-tumoral environment through similar mechanisms. Additionally, different cell types, including certain myeloid-lineage cells such as DCs, express IDO1 in response to IFNγ stimulation [48].

We observed augmented tumor infiltrating CD14 + immune cells (internal and TCGA cohorts). CD14 antigen is highly expressed in monocytes, macrophages, and other myeloid cells. Activating CD14 in tumor infiltrating immune cells can enhance cancer-related inflammation and immunosurveillance or promote an immunosuppressive environment that facilitates tumor progression [49]. MDSCs suppress NK cell activity, undermining the efficacy of NK cell-based immunotherapy in HNSC. TAMs, frequently detected in HNSC, are recruited into tumors with a hypoxic environment. A higher rate of infiltrated neutrophils was found in tumor samples from both cohorts. Myeloid cells, including macrophages, MDSCs, DCs, and neutrophils, promote an immunosuppressive TME by secreting multiple factors, such as IL-10, TGFβ1, PD-L1, ARG1 [50]. The *IL10* and *TGFB1* genes were upregulated in TCGA-OSCC samples, *CD274* (*PD-L1*) was not differentially expressed, and *ARG1* was downregulated. IL-10 inhibits antigen presentation by antigen-presenting cells, such as macrophages and DCs, regulating the differentiation of Tregs and leading to the resistance to cytotoxic T-cell action upon tumor cells [51]. Hypoxic stress induces immunosuppressive molecules like IL-10 and TGFβ1. This might be the case with the TCGA-OSCC samples, in which we verified the upregulation of *HIF1A*, a subunit of the transcription factor HIF-1.

On top of favoring OSCC tumorigenesis by dysregulating the expression of oncogenes and tumor suppressor genes, aberrant DNA methylation affects immune response-related genes, which have been associated with OSCC prognosis and response to therapy [52–54]. Basu and colleagues reported a set of hypomethylated and overexpressed genes implicated in immune response and associated with better survival in OSCC [55]. Herein, we detected the differential methylation of *MALAT1* (metastasis associated lung adenocarcinoma transcript 1), *HOTAIR*, *H19*, *MIR155HG*, *MEG3*, and *HULC*, which were previously associated with immune cells functions [31].

A cross-validation analysis comparing the results of the internal cohort with TCGA-OSCC DNA methylation and RNA-seq data was performed. All the lncRNAs, except *MALAT1* and *HULC* were differentially expressed in TCGA-OSCC. The remaining four lncRNAs (*HOTAIR, H19*, *MIR155HG*, and *MEG3*) exhibited the same trend in the methylation

status of tumor samples in both cohorts. Three selected lncRNAs (*MIR155HG, MEG3,* and *WFDC21P*) were evaluated by BS-pyrosequencing, and the hypomethylation was confirmed in the internal and external OSCC cohorts. Earlier evidence showed that *MEG3* expression was modulated by DNA methylation in OSCC [56]. *MEG3* sponges the microRNA-17 and indirectly upregulates the transcription factor retinoid acid receptor-related orphan receptor gamma t (RORγt), encoded by RAR related orphan receptor C (*RORC*) [57]. RORγt regulates the differentiation of CD4 + T cells into T helper 17 suggesting that *MEG3* is a promising immunological target [58]. Previous evidence links *MEG3* to the regulation of TGF-β pathway genes by interacting with EZH2 (histone methyltransferase enhancer of zeste 2 polycomb repressive complex 2 subunit), the catalytic subunit of polycomb repressive complex 2 [59]. Through this interaction, *MEG3* induces the deposition of repressive histone marks and inhibits the transcription of *TGFBR1* (transforming growth factor beta receptor 1), *TGFB2* (transforming growth factor beta 2), and *SMAD2* (SMAD family member 2) [60].

The second lncRNA confirmed as altered in our dataset, *MIR155HG,* showed a negative correlation between DNA methylation and expression levels in gliomas [61]. The authors showed an association between *MIR155HG* expression and immunosuppressive factors secreted by TAMs, MDSCs, and TANs (tumor-associated neutrophils), stromal cell infiltration, inflammatory activities, and immune checkpoints (such as TIM-3, PD-1, B7-H3, PD-L1, CTLA4, and PD-L2). *MALAT1*, *HOTAIR*, *H19*, and *MIR155HG* have been related to several macrophage-associated functions. *MALAT1* and *HULC* participate in Treg differentiation, and *MEG3* contributes to the modulation of Treg/T helper 17 balance [57,62–67]. Considering that lncRNAs are involved in several immune functions and their regulatory interaction with protein-coding genes are involved in OSCC hallmarks, including immune evasion, it seems reasonable to suppose that the aberrantly methylated lncRNAs that we detected herein contribute to shaping the TME immune component in OSCC and are potential immunotherapeutic targets.

Tumor-associated myeloid cells, namely TAMs and TANs, can play tumor-promoting and anti-tumor roles depending on their state of functional activation [68]. Macrophages are generally classified into M1 and M2 subtypes, according to these functions. Certain molecular stimuli can shift TAM polarization from an M1-like, anti-tumor state to an M2-like, immunosuppressive state. TAN activity can also switch between N1 and N2, anti-tumor and protumor states, respectively. Although the methylation signature that we used for *in silico* deconvolution does not allow us to distinguish macrophages from other monocyte-lineage cells or between their activation states, TAMs are recognized as the major immune cell population in OSCC [69]. Interestingly, previous studies described the lncRNAs *MIR155HG* and *HOTAIR* associated with macrophage polarization and inflammatory response regulation [62,65]. Both lncRNAs were upregulated and correlated with DNA methylation in OSCC samples. *MIR155HG* was previously implicated in macrophage polarization by regulating TNF, IL1B, IL10, and IL12 (interleukin 12) [65]. *HOTAIR* is required for pathogen-induced activation of cytokine expression and pro-inflammatory response in macrophages [62]. Thus, the overexpressed lncRNAs might be active players in regulating the immune response in the complex OSCC TME herein described. *MIR155HG* and *HOTAIR* seem to harness TAMs infiltration to promote anti-tumor responses. On the other hand, *H19*, which is involved in macrophage activation, was also found to be hypermethylated and downregulated in OSCC samples; therefore, could serve as a target to enhance M1 polarization [64].

Epigenetic and tumor immune microenvironment abnormalities might concur in promoting OSCC heterogeneity at molecular and clinical levels and be explored for epi-immunotherapy. Growing evidence shows that epigenetic drugs can be synergistically combined with immune therapy to improve response to cancer treatment [70]. Our study revealed immune factors (Supplementary Figure 5) with potential relevance in OSCC treatment.

5. Conclusions

Using DNA methylation data, we demonstrated that the immune component in OSCC is highly intricate and complex. The dominant cell infiltrates show a functional plasticity with transitions between anti-tumor and immunosuppressive states in response to multiple molecular stimuli. We detected differentially methylated and expressed lncRNAs that could tilt this delicate balance in favor of anti-tumor response. This set of lncRNAs was previously associated with diverse functions in macrophages, Tregs, and DCs. The aberrant DNA methylation in OSCC contributed to the tumor immune microenvironment characterization and might be harnessed to fine-tune TME regulatory factors, such as immune-related lncRNAs, for prognostic and therapeutic purposes.

Ethics approval and consent to participate

The study was conducted according to the guidelines of the Declaration of Helsinki and approved by the Research Ethics Committee of the A.C.Camargo Cancer Center (Protocol #1876/14). Informed consent was obtained from all subjects involved in the study.

Funding

This work was supported by grants from Region of Southern Denmark Research Fund, National Institute of Science and Technology in Oncogenomics (INCITO - Fundação de Amparo à Pesquisa do Estado de São Paulo - FAPESP 2008/57887–9 and Conselho Nacional de Desenvolvimento Científico e Tecnológico - CNPq 573589/08–9). NC was granted with scholarship from the Brazilian Federal Agency for Support and Evaluation of Graduate Education (CAPES), within the scope of the Program CAPES-PrInt (process number 88887.310463/2018-00, mobility number 88887.570391/2020-00).

CRediT authorship contribution statement

Naiade Calanca: Methodology, Validation, Formal analysis, Writing – original draft, Writing – review & editing. **Ana Lucia Noronha Francisco:** Conceptualization, Investigation, Methodology, Writing – review & editing. **Daniela Bizinelli:** Formal analysis, Validation, Writing – review & editing. **Hellen Kuasne:** Methodology, Formal analysis, Writing – review & editing. **Mateus Camargo Barros Filho:** Formal analysis, Writing – review & editing. **Bianca Campos Troncarelli Flores:** Validation, Writing – review & editing. **Clóvis Antonio Lopes Pinto:** Investigation, Writing – review & editing. **Claudia Aparecida Rainho:** Formal analysis, Supervision, Writing – review & editing. **Milena Botelho Pereira Soares:** Validation, Writing – review & editing. **Fabio Albuquerque Marchi:** Formal analysis, Writing – review & editing. **Luiz Paulo Kowalski:** Conceptualization, Investigation, Resources, Data curation, Supervision, Funding acquisition, Writing – review & editing. **Silvia Regina Rogatto:** Conceptualization, Formal analysis, Resources, Data curation, Supervision, Funding acquisition, Writing – original draft, Writing – review & editing, Project administration.

Declaration of Competing Interest

The authors declare that they have no known competing financial interests or personal relationships that could have appeared to influence the work reported in this paper.

Data Availability

The dataset generated during the current study has been deposited in

NCBI's Gene Expression Omnibus (GEO) database and is accessible through GSE234379.

Acknowledgements

The authors would like to thank the patients for accepting to participate of the study and the Nucleic Acid Bank of A.C. Camargo Cancer Center (São Paulo, Brazil) for sample processing. The authors are grateful to Mariana Bizarro dos Reis and Tarsila Guimarães Vieira da Silva for the assistance during the experiments.

Appendix A. Supporting information

Supplementary data associated with this article can be found in the online version at doi:10.1016/j.biopha.2023.115559.

References

[1] D.E. Johnson, B. Burtness, C.R. Leemans, V.W.Y. Lui, J.E. Bauman, J.R. Grandis, Head and neck squamous cell carcinoma, Nat. Rev. Dis. Prim. 6 (2020), https://doi.org/10.1038/s41572-020-00224-3.
[2] C. Rivera, Essentials of oral cancer, Int. J. Clin. Exp. Pathol. 8 (2015) 11884–11894. ⟨http://www.ncbi.nlm.nih.gov/pubmed/26617944⟩.
[3] C. de Martel, D. Georges, F. Bray, J. Ferlay, G.M. Clifford, Global burden of cancer attributable to infections in 2018: a worldwide incidence analysis, Lancet Glob. Health 8 (2020) e180–e190, https://doi.org/10.1016/S2214-109X(19)30488-7.
[4] V.M. Patil, V. Noronha, A. Joshi, A. Abhyankar, N. Menon, S. Dhumal, K. Prabhash, Beyond conventional chemotherapy, targeted therapy and immunotherapy in squamous cell cancer of the oral cavity, Oral. Oncol. 105 (2020), https://doi.org/10.1016/j.oraloncology.2020.104673.
[5] Y. Huang, Y. Lan, Z. Zhang, X. Xiao, T. Huang, An update on the immunotherapy for oropharyngeal squamous cell carcinoma, Front Oncol. 12 (2022) 1–10, https://doi.org/10.3389/fonc.2022.800315.
[6] D. Peng, I. Kryczek, N. Nagarsheth, L. Zhao, S. Wei, W. Wang, Y. Sun, E. Zhao, L. Vatan, W. Szeliga, J. Kotarski, R. Tarkowski, Y. Dou, K. Cho, S. Hensley-Alford, A. Munkarah, R. Liu, W. Zou, Epigenetic silencing of TH1-type chemokines shapes tumour immunity and immunotherapy, Nature 527 (2015) 249–253, https://doi.org/10.1038/nature15520.
[7] A. Elmusrati, J. Wang, C.Y. Wang, Tumor microenvironment and immune evasion in head and neck squamous cell carcinoma, Int J. Oral. Sci. 13 (1) (2021) 11, https://doi.org/10.1038/s41368-021-00131-7.
[8] P. Diao, Y. Jiang, Y. Li, X. Wu, J. Li, C. Zhou, L. Jiang, W. Zhang, E. Yan, P. Zhang, X. Ding, H. Wu, H. Yuan, J. Ye, X. Song, L. Wan, Y. Wu, H. Jiang, Y. Wang, J. Cheng, Immune landscape and subtypes in primary resectable oral squamous cell carcinoma: prognostic significance and predictive of therapeutic response, J. Immunother. Cancer 9 (2021), e002434, https://doi.org/10.1136/jitc-2021-002434.
[9] J. Galon, D. Bruni, Approaches to treat immune hot, altered and cold tumours with combination immunotherapies, Nat. Rev. Drug Discov. 18 (2019) 197–218, https://doi.org/10.1038/s41573-018-0007-y.
[10] S.-N. Huang, G.-S. Li, X.-G. Zhou, X.-Y. Chen, Y.-X. Yao, X.-G. Zhang, Y. Liang, M.-X. Li, G. Chen, Z.-G. Huang, Y.-W. Dang, J. Li, P. Li, X.-Z. Tang, M.-H. Rong, Identification of an immune score-based gene panel with prognostic power for oral squamous cell carcinoma, Med. Sci. Monit. 26 (2020), https://doi.org/10.12659/MSM.922854.
[11] S. Zhang, H. Yu, J. Li, L. Zhao, L. Tan, Q. Song, C. Sun, Identification of prognostic and tumor microenvironment by shelterin complex-related signatures in oral squamous cell carcinoma, Oxid. Med. Cell Longev. 2022 (2022) 1–35, https://doi.org/10.1155/2022/6849304.
[12] Y. Zhao, D. Chen, J. Yin, J. Xie, C. Sun, M. Lu, Comprehensive analysis of tumor immune microenvironment characteristics for the prognostic prediction and immunotherapy of oral squamous cell carcinoma, Front Genet 13 (2022), https://doi.org/10.3389/fgene.2022.788580.
[13] D. Hanahan, Hallmarks of cancer: new dimensions, Cancer Discov. 12 (2022) 31–46, https://doi.org/10.1158/2159-8290.CD-21-1059.
[14] L. Villanueva, D. Álvarez-Errico, M. Esteller, The contribution of epigenetics to cancer immunotherapy, Trends Immunol. 41 (2020) 676–691, https://doi.org/10.1016/j.it.2020.06.002.
[15] Y. Zhou, W. Sun, Z. Qin, S. Guo, Y. Kang, S. Zeng, L. Yu, LncRNA regulation: new frontiers in epigenetic solutions to drug chemoresistance, Biochem Pharm. 189 (2021), https://doi.org/10.1016/j.bcp.2020.114228.
[16] D.C. Peltier, A. Roberts, P. Reddy, LNCing RNA to immunity, Trends Immunol. 43 (2022) 478–495, https://doi.org/10.1016/j.it.2022.04.002.
[17] M.K. Atianand, D.R. Caffrey, K.A. Fitzgerald, Immunobiology of long noncoding RNAs, Annu Rev. Immunol. 35 (2017) 177–198, https://doi.org/10.1146/annurev-immunol-041015-055459.
[18] T.J. Morris, L.M. Butcher, A. Feber, A.E. Teschendorff, A.R. Chakravarthy, T. K. Wojdacz, S. Beck, ChAMP: 450k chip analysis methylation pipeline, Bioinformatics 30 (2014) 428–430, https://doi.org/10.1093/bioinformatics/btt684.
[19] Y. Tian, T.J. Morris, A.P. Webster, Z. Yang, S. Beck, A. Feber, A.E. Teschendorff, ChAMP: updated methylation analysis pipeline for Illumina BeadChips, Bioinformatics 33 (2017) 3982–3984, https://doi.org/10.1093/bioinformatics/btx513.
[20] A.E. Teschendorff, F. Marabita, M. Lechner, T. Bartlett, J. Tegner, D. Gomez-Cabrero, S. Beck, A beta-mixture quantile normalization method for correcting probe design bias in Illumina Infinium 450 k DNA methylation data, Bioinformatics 29 (2013) 189–196, https://doi.org/10.1093/bioinformatics/bts680.
[21] M.E. Ritchie, B. Phipson, D. Wu, Y. Hu, C.W. Law, W. Shi, G.K. Smyth, limma powers differential expression analyses for RNA-sequencing and microarray studies, Nucleic Acids Res 43 (2015), https://doi.org/10.1093/nar/gkv007 e47–e47.
[22] Cancer Genome Atlas Network, Comprehensive genomic characterization of head and neck squamous cell carcinomas, Nature 517 (2015) 576–582, https://doi.org/10.1038/nature14129.
[23] M.J. Goldman, B. Craft, M. Hastie, K. Repečka, F. McDade, A. Kamath, A. Banerjee, Y. Luo, D. Rogers, A.N. Brooks, J. Zhu, D. Haussler, Visualizing and interpreting cancer genomics data via the Xena platform, Nat. Biotechnol. 38 (2020) 675–678, https://doi.org/10.1038/s41587-020-0546-8.
[24] A. Colaprico, T.C. Silva, C. Olsen, L. Garofano, C. Cava, D. Garolini, T.S. Sabedot, T. M. Malta, S.M. Pagnotta, I. Castiglioni, M. Ceccarelli, G. Bontempi, H. Noushmehr, TCGAbiolinks: an R/Bioconductor package for integrative analysis of TCGA data, Nucleic Acids Res 44 (2016), https://doi.org/10.1093/nar/gkv1507.
[25] M. Mounir, M. Lucchetta, T.C. Silva, C. Olsen, G. Bontempi, X. Chen, H. Noushmehr, A. Colaprico, E. Papaleo, New functionalities in the TCGAbiolinks package for the study and integration of cancer data from GDC and GTEx, PLoS Comput. Biol. 15 (2019), e1006701, https://doi.org/10.1371/journal.pcbi.1006701.
[26] S. Durinck, Y. Moreau, A. Kasprzyk, S. Davis, B. de Moor, A. Brazma, W. Huber, BioMart and Bioconductor: a powerful link between biological databases and microarray data analysis, Bioinformatics 21 (2005) 3439–3440, https://doi.org/10.1093/bioinformatics/bti525.
[27] M.I. Love, W. Huber, S. Anders, Moderated estimation of fold change and dispersion for RNA-seq data with DESeq2, Genome Biol. 15 (2014), 550, https://doi.org/10.1186/s13059-014-0550-8.
[28] A. Chakravarthy, A. Furness, K. Joshi, E. Ghorani, K. Ford, M.J. Ward, E.V. King, M. Lechner, T. Marafioti, S.A. Quezada, G.J. Thomas, A. Feber, T.R. Fenton, Pan-cancer deconvolution of tumour composition using DNA methylation, Nat. Commun. 9 (2018), https://doi.org/10.1038/s41467-018-05570-1.
[29] F. Seifuddin, K. Singh, A. Suresh, J.T. Judy, Y.-C. Chen, V. Chaitankar, I. Tunc, X. Ruan, P. Li, Y. Chen, H. Cao, R.S. Lee, F.S. Goes, P.P. Zandi, M.S. Jafri, M. Pirooznia, lncRNAKB, a knowledgebase of tissue-specific functional annotation and trait association of long noncoding RNA, Sci. Data 7 (2020), 326, https://doi.org/10.1038/s41597-020-00659-z.
[30] Z. Gu, R. Eils, M. Schlesner, Complex heatmaps reveal patterns and correlations in multidimensional genomic data, Bioinformatics 32 (2016) 2847–2849, https://doi.org/10.1093/bioinformatics/btw313.
[31] S. Khan, M. Masood, H. Gaur, S. Ahmad, M. Ali, Long non-coding RNA: an immune cells perspective, Life Sci. 271 (2021), 119152, https://doi.org/10.1016/j.lfs.2021.119152.
[32] D. Goksuluk, S. Korkmaz, G. Zararsiz, A.E. Karaagaoglu, easyROC: an interactive web-tool for ROC curve analysis using R language environment, R. J. 8 (2016) 213, https://doi.org/10.32614/RJ-2016-042.
[33] P.J. Hsu, K. Yan, H. Shi, E. Izumchenko, N. Agrawal, Molecular biology of oral cavity squamous cell carcinoma, Oral. Oncol. 102 (2020), 104552, https://doi.org/10.1016/j.oraloncology.2019.104552.
[34] P.V. Jithesh, J.M. Risk, A.G. Schache, J. Dhanda, B. Lane, T. Liloglou, R.J. Shaw, The epigenetic landscape of oral squamous cell carcinoma, Br. J. Cancer (2013) 370–379, https://doi.org/10.1038/bjc.2012.568.
[35] M. Esteller, Cancer epigenomics: DNA methylomes and histone-modification maps, Nat. Rev. Genet 8 (2007) 286–298, https://doi.org/10.1038/nrg2005.
[36] E. Alspach, D.M. Lussier, R.D. Schreiber, Interferon γ and its important roles in promoting and inhibiting spontaneous and therapeutic cancer immunity, Cold Spring Harb. Perspect. Biol. 11 (2019), https://doi.org/10.1101/cshperspect.a028480.
[37] I. Voskoboinik, J.C. Whisstock, J.A. Trapani, Perforin and granzymes: function, dysfunction and human pathology, Nat. Rev. Immunol. 15 (2015) 388–400, https://doi.org/10.1038/nri3839.
[38] A.M. Abel, C. Yang, M.S. Thakar, S. Malarkannan, Natural killer cells: development, maturation, and clinical utilization, Front Immunol. 9 (2018), https://doi.org/10.3389/fimmu.2018.01869.
[39] R. Sales de Sá, M. Miranda Galvis, B.A.L.A. Mariz, A.A. Leite, L. Schultz, O. P. Almeida, A.R. Santos-Silva, C.A.L. Pinto, P.A. Vargas, K.J. Gollob, L.P. Kowalski, Increased tumor immune microenvironment CD3+ and CD20+ lymphocytes predict a better prognosis in oral tongue squamous cell carcinoma, Front Cell Dev. Biol. 8 (2021) 1–13, https://doi.org/10.3389/fcell.2020.622161.
[40] Z. Huang, N. Xie, H. Liu, Y. Wan, Y. Zhu, M. Zhang, Y. Tao, H. Zhou, X. Liu, J. Hou, C. Wang, The prognostic role of tumour-infiltrating lymphocytes in oral squamous cell carcinoma: a meta-analysis, J. Oral. Pathol. Med. 48 (2019) 788–798, https://doi.org/10.1111/jop.12927.
[41] X.M. Lao, Y.J. Liang, Y.X. Su, S.E. Zhang, X. Zhou, G.Q. Liao, Distribution and significance of interstitial fibrosis and stroma-infiltrating B cells in tongue squamous cell carcinoma, Oncol. Lett. 11 (2016) 2027–2034, https://doi.org/10.3892/ol.2016.4184.
[42] W.H. Fridman, M. Meylan, F. Petitprez, C.M. Sun, A. Italiano, C. Sautès-Fridman, B cells and tertiary lymphoid structures as determinants of tumour immune

contexture and clinical outcome, Nat. Rev. Clin. Oncol. 19 (2022) 441–457, https://doi.org/10.1038/s41571-022-00619-z.
[43] X. Zhou, Y.X. Su, X.M. Lao, Y.J. Liang, G.Q. Liao, CD19+IL-10+ regulatory B cells affect survival of tongue squamous cell carcinoma patients and induce resting CD4 + T cells to CD4+Foxp3+ regulatory T cells, Oral. Oncol. 53 (2016) 27–35, https://doi.org/10.1016/j.oraloncology.2015.11.003.
[44] A.A.M. Adil, A.K. Bommanabonia, A. Vaithy, S. Kumar, M. Waseem, S. Jamal, N. Ahmed, Differential expression of Helios, Neuropilin-1 and FoxP3 in head and neck squamous cell carcinoma (HNSCC) patients, 3 Biotech 9 (2019), 178, https://doi.org/10.1007/s13205-019-1707-7.
[45] J. Wang, R. Gong, C. Zhao, K. lei, X. Sun, H. Ren, Human FOXP3 and tumor microenvironment, Immunology (2022) 1–8, https://doi.org/10.1111/imm.13520.
[46] C.A. Opitz, L.F. Somarribas Patterson, S.R. Mohapatra, D.L. Dewi, A. Sadik, M. Platten, S. Trump, The therapeutic potential of targeting tryptophan catabolism in cancer, Br. J. Cancer 122 (2020) 30–44, https://doi.org/10.1038/s41416-019-0664-6.
[47] F. Fallarino, U. Grohmann, S. You, B.C. McGrath, D.R. Cavener, C. Vacca, C. Orabona, R. Bianchi, M.L. Belladonna, C. Volpi, P. Santamaria, M.C. Fioretti, P. Puccetti, The combined effects of tryptophan starvation and tryptophan catabolites down-regulate T cell receptor ζ-chain and induce a regulatory phenotype in naive T cells, J. Immunol. 176 (2006) 6752–6761, https://doi.org/10.4049/jimmunol.176.11.6752.
[48] A.L. Mellor, D.H. Munn, IDO expression by dendritic cells: tolerance and tryptophan catabolism, Nat. Rev. Immunol. 4 (2004) 762–774, https://doi.org/10.1038/nri1457.
[49] Z. Wu, Z. Zhang, Z. Lei, P. Lei, CD14: Biology and role in the pathogenesis of disease, Cytokine Growth Factor Rev. 48 (2019) 24–31, https://doi.org/10.1016/j.cytogfr.2019.06.003.
[50] T.M. Grzywa, A. Sosnowska, P. Matryba, Z. Rydzynska, M. Jasinski, D. Nowis, J. Golab, Myeloid cell-derived arginase in cancer immune response, Front. Immunol. 11 (2020), https://doi.org/10.3389/fimmu.2020.00938.
[51] N. Kondoh, M. Mizuno-Kamiya, N. Umemura, E. Takayama, H. Kawaki, K. Mitsudo, Y. Muramatsu, S. Sumitomo, Immunomodulatory aspects in the progression and treatment of oral malignancy, Jpn. Dent. Sci. Rev. 55 (2019) 113–120, https://doi.org/10.1016/j.jdsr.2019.09.001.
[52] S.Y. Kim, Y.K. Han, J.M. Song, C.H. Lee, K. Kang, J.M. Yi, H.R. Park, Aberrantly hypermethylated tumor suppressor genes were identified in oral squamous cell carcinoma (OSCC), Clin. Epigenet. 11 (2019), https://doi.org/10.1186/s13148-019-0715-0.
[53] X. Zhang, H. Feng, D. Li, S. Liu, N. Amizuka, M. Li, Identification of differentially expressed genes induced by aberrant methylation in oral squamous cell carcinomas using integrated Bioinformatic analysis, Int. J. Mol. Sci. 19 (2018) 1–15, https://doi.org/10.3390/ijms19061698.
[54] C. Shi, S. Liu, X. Tian, C. Miao, R. Wang, X. Ma, X. Wang, Y. Cao, Prognostic and therapeutic prediction by screening signature combinations from transcriptome–methylome interactions in oral squamous cell carcinoma, Sci. Rep. 12 (2022), 11400, https://doi.org/10.1038/s41598-022-15534-7.
[55] B. Basu, J. Chakraborty, A. Chandra, A. Katarkar, J.R.K. Baldevbhai, D. Dhar Chowdhury, J.G. Ray, K. Chaudhuri, R. Chatterjee, Genome-wide DNA methylation profile identified a unique set of differentially methylated immune genes in oral squamous cell carcinoma patients in India, Clin. Epigenet. 9 (1) (2017) 15, https://doi.org/10.1186/s13148-017-0314-x.
[56] Z. Liu, C. Wu, N. Xie, P. Wang, Long non-coding RNA MEG3 inhibits the proliferation and metastasis of oral squamous cell carcinoma by regulating the WNT/β-catenin signaling pathway, Oncol. Lett. 14 (2017) 4053–4058, https://doi.org/10.3892/ol.2017.6682.
[57] Y. ying Qiu, Y. Wu, M. jie Lin, T. Bian, Y. long Xiao, C. Qin, LncRNA-MEG3 functions as a competing endogenous RNA to regulate Treg/Th17 balance in patients with asthma by targeting microRNA-17/ RORγt, Biomed. Pharmacother. 111 (2019) 386–394, https://doi.org/10.1016/j.biopha.2018.12.080.
[58] G.R. Lee, The balance of th17 versus treg cells in autoimmunity, Int. J. Mol. Sci. 19 (2018), https://doi.org/10.3390/ijms19030730.
[59] L. Zhang, F. Zhao, W. Li, G. Song, V. Kasim, S. Wu, The biological roles and molecular mechanisms of long non-coding RNA MEG3 in the hallmarks of cancer, Cancers (Basel) 14 (2022), https://doi.org/10.3390/cancers14246032.
[60] T. Mondal, S. Subhash, R. Vaid, S. Enroth, S. Uday, B. Reinius, S. Mitra, A. Mohammed, A.R. James, E. Hoberg, A. Moustakas, U. Gyllensten, S.J.M. Jones, C.M. Gustafsson, A.H. Sims, F. Westerlund, E. Gorab, C. Kanduri, MEG3 long noncoding RNA regulates the TGF-β pathway genes through formation of RNA-DNA triplex structures, Nat. Commun. 6 (2015), https://doi.org/10.1038/ncomms8743.
[61] X. Wu, Q. Wan, J. Wang, P. Hou, Q. Zhang, Q. Wang, X. Lu, Epigenetic activation of lncRNA MIR155HG mediated by promoter hypomethylation and SP1 is correlated with immune infiltration in glioma, Onco Targets Ther. Volume 15 (2022) 219–235, https://doi.org/10.2147/OTT.S349078.
[62] M. Obaid, S.M.N. Udden, P. Deb, N. Shihabeddin, M.H. Zaki, S.S. Mandal, LncRNA HOTAIR regulates lipopolysaccharide-induced cytokine expression and inflammatory response in macrophages, Sci. Rep. 8 (2018), https://doi.org/10.1038/s41598-018-33722-2.
[63] J.-L. Pang, J.-W. Wang, P.-Y. Hu, J.-S. Jiang, C. Yu, HOTAIR alleviates ox-LDL-induced inflammatory response in Raw264.7 cells via inhibiting NF-κB pathway. Eur. Rev. Med. Pharm. Sci. 22 (2018) 6991–6998, https://doi.org/10.26355/eurrev_201810_16170.
[64] X. Li, R. Liu, Y. Wang, W. Zhu, D. Zhao, X. Wang, H. Yang, E.C. Gurley, W. Chen, P. B. Hylemon, H. Zhou, Cholangiocyte-derived exosomal lncRNA H19 promotes macrophage activation and hepatic inflammation under cholestatic conditions, Cells 9 (2020), https://doi.org/10.3390/cells9010190.
[65] N. Li, Y. Liu, J. Cai, LncRNA MIR155HG regulates M1/M2 macrophage polarization in chronic obstructive pulmonary disease, Biomed. Pharmacother. 117 (2019), https://doi.org/10.1016/j.biopha.2019.109015.
[66] F. Masoumi, S. Ghorbani, F. Talebi, W.G. Branton, S. Rajaei, C. Power, F. Noorbakhsh, Malat1 long noncoding RNA regulates inflammation and leukocyte differentiation in experimental autoimmune encephalomyelitis, J. Neuroimmunol. 328 (2019) 50–59, https://doi.org/10.1016/j.jneuroim.2018.11.013.
[67] J. Zhao, Y. Fan, K. Wang, X. Ni, J. Gu, H. Lu, Y. Lu, L. Lu, X. Dai, X. Wang, LncRNA HULC affects the differentiation of Treg in HBV-related liver cirrhosis, Int. Immunopharmacol. 28 (2015) 901–905, https://doi.org/10.1016/j.intimp.2015.04.028.
[68] A. Mantovani, F. Marchesi, S. Jaillon, C. Garlanda, P. Allavena, Tumor-associated myeloid cells: diversity and therapeutic targeting, Cell Mol. Immunol. 18 (2021) 566–578, https://doi.org/10.1038/s41423-020-00613-4.
[69] E.M. Kalogirou, K.I. Tosios, P.F. Christopoulos, The role of macrophages in oral squamous cell carcinoma, Front Oncol. 11 (2021), https://doi.org/10.3389/fonc.2021.611115.
[70] Y. Xu, P. Li, Y. Liu, D. Xin, W. Lei, A. Liang, W. Han, W. Qian, Epi-immunotherapy for cancers: rationales of epi-drugs in combination with immunotherapy and advances in clinical trials, Cancer Commun. 42 (2022) 493–516, https://doi.org/10.1002/cac2.12313.